Table 2
Echocardiographic and hemodynamic data

	Control	BPS
AWT diastole (mm)	0.62 ± 0.04	0.74 ± 0.05
AW thickening (%)	17 ± 3	34 ± 6*
PWT diastole (mm)	1.55 ± 0.07	1.70 ± 0.04
PW thickening (%)	43 ± 4	49 ± 3
Heart rate (bpm)	458 ± 7	471 ± 10
Mean arterial pressure (mmHg)	103 ± 5	115 ± 4
LV systolic pressure (mmHg)	113 ± 4	127 ± 5*
LV diastolic wall stress (kdyne/cm^2)	24 ± 4	5 ± 1**
LV systolic wall stress (kdyne/cm^2)	267 ± 18	225 ± 14

AWT, anterior wall thickness; AW, anterior wall; PWT, posterior wall thickness; PW, posterior wall. Data are expressed as means ± SEM. *$p < 0.05$, **$p < 0.01$ vs. Control group.

Mobilization of bone marrow cells

RT-PCR demonstrated that IP receptor mRNA was expressed in bone marrow cells (Fig. 3A), indicating a direct effect of BPS on these cells. Three-day administration of BPS significantly increased the number of peripheral blood mononuclear cells compared to saline administration (Fig. 3B). Administration of BPS markedly increased the number of circulating progenitor cells such as CD34-positive cells and c-kit-positive cells (Fig. 3C and D). BPS also increased the number of CD45-positive hematopoietic lineage cells (Fig. 3E).

BPS-induced neovascularization

Chimeric rats with GFP-expressing bone marrow were used to assess recruitment of bone marrow cells. Four weeks after coronary ligation, bone marrow-derived GFP-positive cells were incorporated predominantly into the infarcted region and its border zone (Fig. 4A), while these cells were rarely detected in the noninfarcted myocardium. Some of the GFP-positive cells stained for vWF and formed vascular structures. Semi-quantitative analysis demonstrated that the number of GFP-positive cells in the myocardium was significantly greater in the BPS group than in the Control group (Fig. 4B). The number of GFP-vWF double-positive cells (bone marrow-derived endothelial cells) in the ischemic myocardium was significantly greater in the BPS group than in the Control group (Fig. 4C). In addition, a small number of GFP-troponin T-double-positive cells were observed in the BPS group (Fig. 4D).

Capillary density

In the peri-infarct area, clustering of relatively small vessels was seen in BPS-treated hearts, which is indicative of recent endothelial regeneration (Fig. 5A). Semi-quantitative analysis also demonstrated that administration of BPS significantly increased the capillary density in the peri-infarct area compared to the Control group (Fig. 5B).

Discussion

In the present study, we demonstrated that treatment with BPS (1) decreased infarct size and improved cardiac structure and function in rats with acute myocardial infarction, (2) increased the number of circulating progenitor cells such as CD34-positive cells and c-kit-positive cells in rats, and (3) increased the number of bone marrow-derived endothelial cells and the capillary density in the ischemic myocardium. These results suggest that BPS may have beneficial effects on ischemic myocardium at least in part through enhancement of neovascularization by mobilizing bone marrow cells.

Earlier studies have reported that prostacyclin has cardioprotective effects in ischemia–reperfusion injury through inhibition of neutrophil activation and migration [25,26]. BPS is also reported to inhibit chemotaxis and superoxide anion production of neutrophils which contribute to tissue damage by releasing tissue destructive lysosomal enzymes [27]. Infusion of BPS has been shown to reduce infarct size in the dog heart with left coronary occlusion by reducing myocardial oxygen demand and by inhibition of the migration of neutrophils [28]. However, these

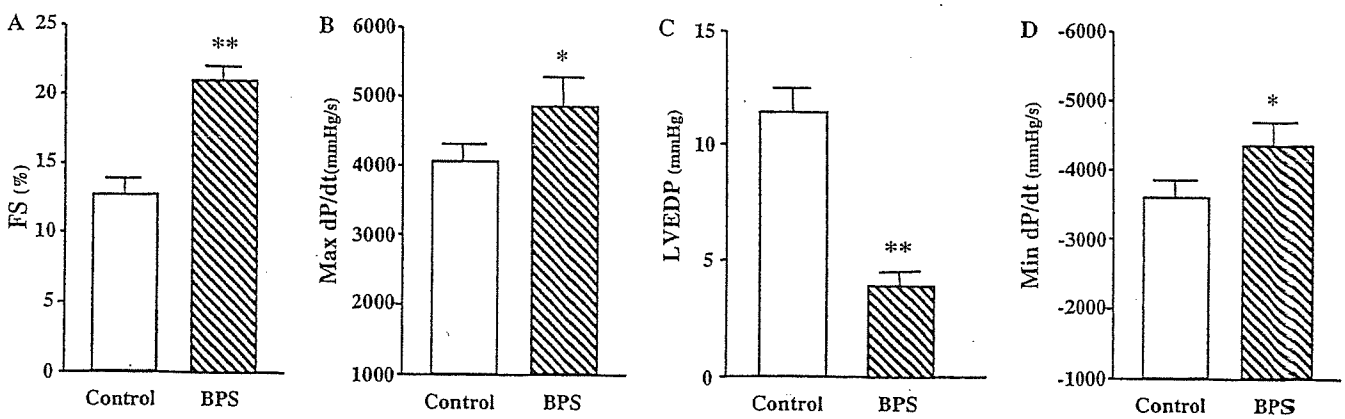

Fig. 2. Cardioprotective effects of BPS on echocardiographic and hemodynamic parameters. FS, fractional shortening; LVEDP, LV end-diastolic pressure; Max and Min dP/dt, maximum and minimum dP/dt. Data are expressed as means ± SEM. *$p < 0.05$, **$p < 0.01$ vs. Control group.

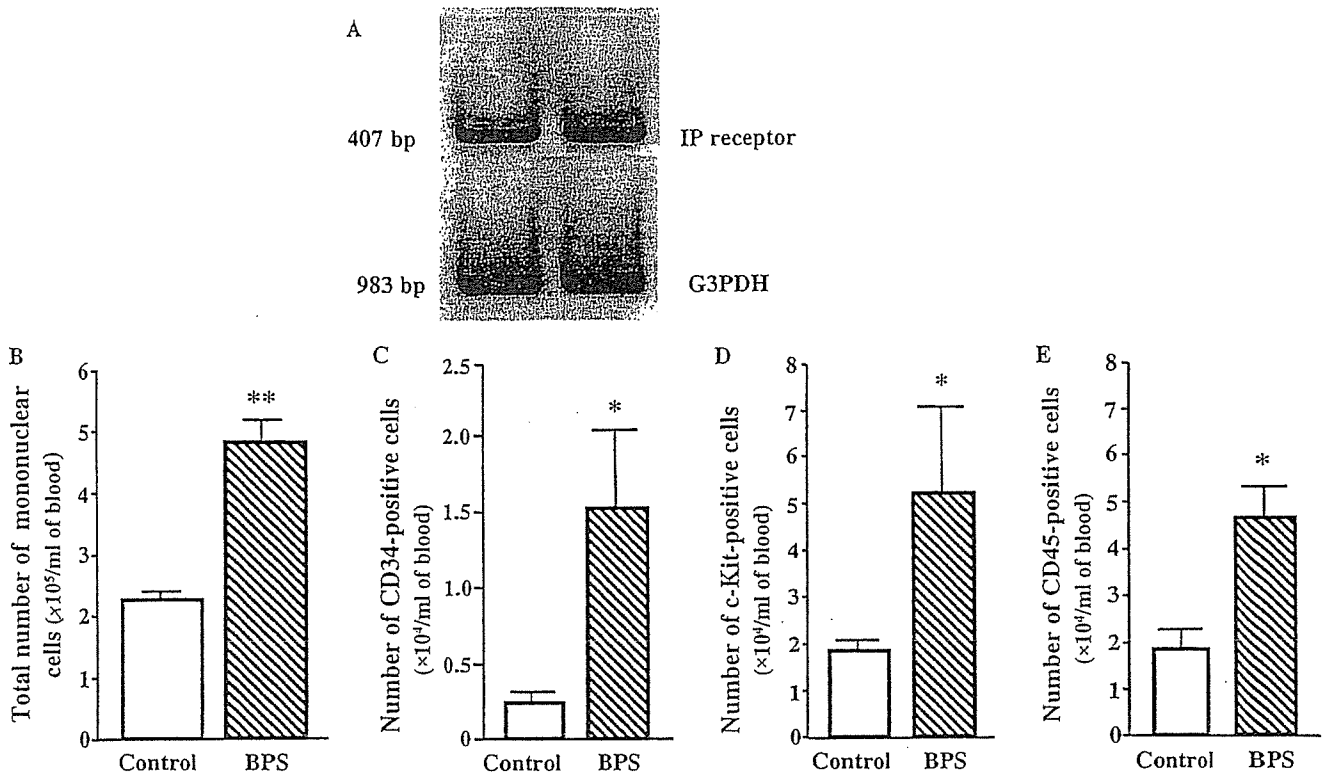

Fig. 3. BPS-induced mobilization of bone marrow cells. (A) Expression of prostacyclin receptor (IP receptor) on bone marrow cells. (B–E) Quantification of BPS-induced MNC mobilization by FACS analysis. Administration of BPS markedly increased the number of circulating progenitor cells such as CD34-positive cells and c-kit-positive cells. BPS also increased the number of CD45-positive hematopoietic lineage cells. Data are expressed as means ± SEM. $^{*}p < 0.05$, $^{**}p < 0.01$ vs. Control group.

biological activities of BPS appear to be insufficient to explain the decrease in infarct size as well as suppression of LV remodeling.

Recent studies have shown that mobilization of bone marrow cells by cytokines promotes myocardial repair and regeneration after acute myocardial infarction [5,6]. In the present study, three-day administration of BPS markedly increased the number of circulating progenitor cells such as CD34-positive cells and c-kit-positive cells in rats. In addition, treatment with BPS enhanced recruitment of bone marrow cells to the ischemic myocardium and increased capillary density in the peri-infarct area. Earlier studies have shown that CD34-positive cells have angiogenic potential to treat ischemic heart [29–31]. Also, another stem cell fraction, c-kit-positive cells have ability to repair ischemic myocardium by differentiating into vascular endothelial cells [32,33]. These findings suggest that administered BPS induces neovascularization partly via enhancement of bone marrow cell mobilization. RT-PCR demonstrated that IP receptor mRNA was expressed in bone marrow cells, indicating a direct effect of BPS on these cells. A recent study has shown that BPS increases eNOS expression in cultured endothelial cells through activation of c-AMP/Protein kinase A signal transduction [19]. Also, earlier studies have shown that eNOS plays essential role in the recruitment of EPCs to the ischemic myocardium [20]. Taken together, administered BPS may act as a potent stimulator of cell mobilization from bone marrow, although further studies are necessary to examine the underlying mechanisms.

In the present study, treatment with BPS significantly attenuated infarct size after myocardial infarction. BPS improved cardiac function and attenuated the development of LV remodeling after acute myocardial infarction, as indicated by increases in LV fractional shortening and maximum dP/dt, and decreases in LVEDP and LVDD. Taken together, BPS may attenuate myocardial infarction through enhancement of neovascularization via modification of bone marrow kinetics. Interestingly, a small fraction of mobilized bone marrow cells expressed cardiac troponin T in the ischemic myocardium in the BPS group, suggesting that BPS may partially contribute to myocardial regeneration after acute myocardial infarction. Earlier studies have demonstrated that BPS has other beneficial effects for ischemic heart disease including anti-thrombotic activity [34], inhibition of reperfusion injury [35], and prevention of coronary spasm [36], and re-stenosis [37]. These findings suggest that administration of BPS may be a promising therapy for acute myocardial infarction.

Granulocyte colony stimulating factor (G-CSF) is currently used agent for mobilization of bone marrow. Infusion of G-CSF after myocardial infarction improves LV function increasing peripheral stem cell fraction [5,38]. A recent clinical trial, however, claimed the G-CSF therapy

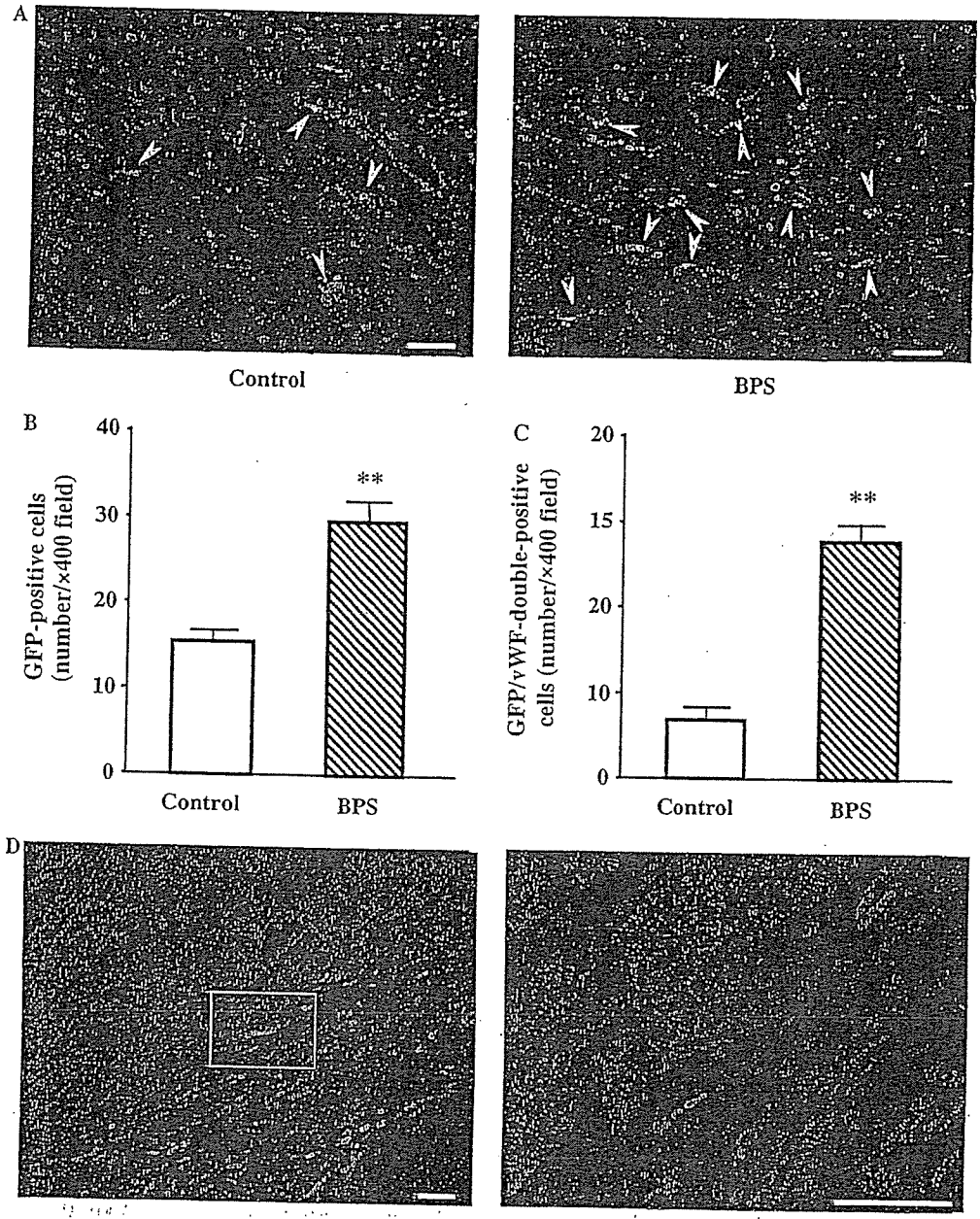

Fig. 4. BPS-induced neovascularization. (A) Representative immunofluorescent images stained with antibodies to von-Willbrand factor (vWF, red) and green fluorescent protein (GFP, green). Nuclei were counterstained with DAPI (blue). (B,C) Semi-quantitative analyses of numbers of GFP-positive cells and GFP-vWF double-positive cells in the peri-infarct area. (D) Representative immunofluorescent image of GFP-positive cells (green) expressing cardiac troponin T (red) observed in the BPS group. Scale bars = 50 μm. Data are expressed as means ± SEM. $^{**}p < 0.01$ vs. Control group.

has serious problem with re-stenosis after recanalization [39]. On the other hand, the safety of BPS has been identified in the treatment of peripheral arterial disease [12,13] and pulmonary arterial hypertension [14,15]. A randomized, controlled clinical trial failed to demonstrate therapeutic potential of prostacyclin for the treatment of severe congestive heart failure [40], which has long discouraged the pursuit of prostacyclin as a therapeutic option for the treatment of acute myocardial infarction. Interestingly, however, double-blinded, randomized, placebo-controlled, large-scale studies showed that treatment with BPS decreased vascular events in patients with peripheral arterial disease [41,42]. Thus, adequate use of BPS for only acute myocardial infarction may have beneficial effects on ischemic myocardium, although further preclinical trials are required to verify the safety and efficacy of BPS.

Conclusion

In summary, administration of BPS improved cardiac structure and function in rats with acute myocardial infarction. This beneficial effect of BPS may be mediated partly by its ability to enhance neovascularization in ischemic myocardium by mobilizing bone marrow cells.

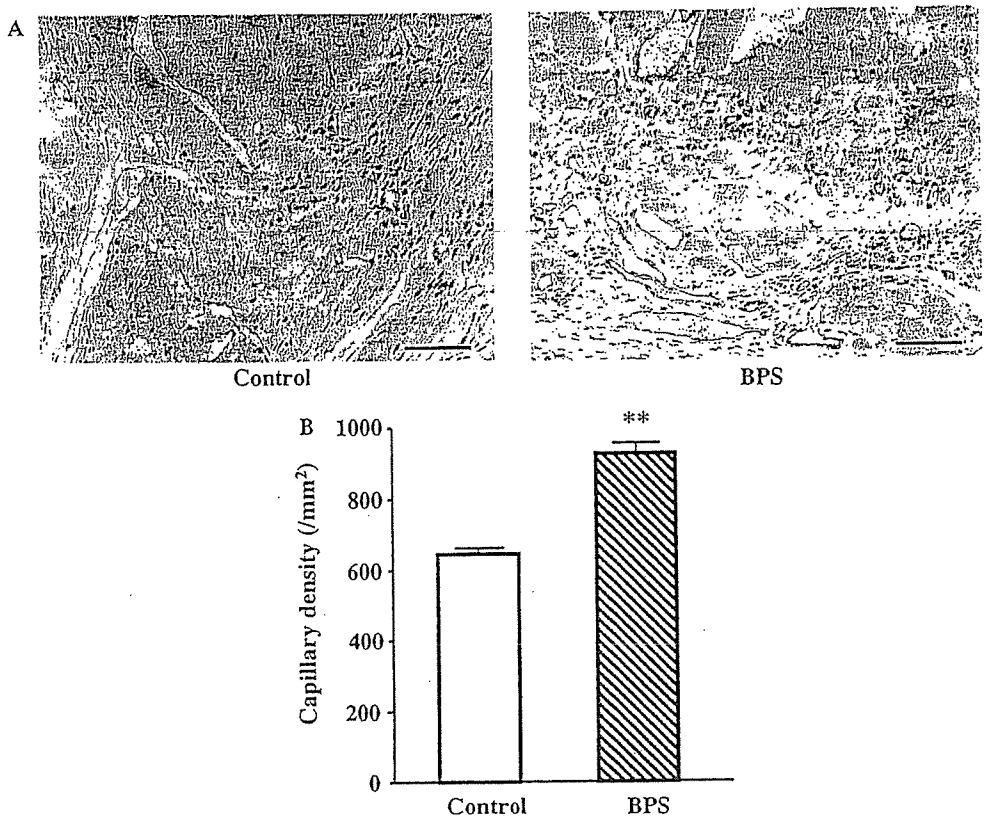

Fig. 5. (A) Representative samples stained with antibody to von Willebrand factor by bright-field DAB. (B) Quantitative analysis of capillary density in peri-infarct area. Administration of BPS increased capillary density by 37%. Scale bars = 50 μm. Data are expressed as means ± SEM. $^{**}p < 0.01$ vs. Control group.

Acknowledgment

This work was supported by research grants for Cardiovascular Disease (16C-6) from the Ministry of Health, Labor and Welfare, and for Japan Vascular Disease Research Foundation.

References

[1] A. Saraste, K. Pulkki, M. Kallajoki, K. Henriksen, M. Parvinen, L.M. Voipio-Pulkki, Apoptosis in human acute myocardial infarction, Circulation 95 (1997) 320–323.
[2] S. Shintani, T. Murohara, H. Ikeda, T. Ueno, T. Honma, A. Katoh, K. Sasaki, T. Shimada, Y. Oike, T. Imaizumi, Mobilization of endothelial progenitor cells in patients with acute myocardial infarction, Circulation 103 (2001) 2776–2779.
[3] D. Orlic, J. Kajstura, S. Chimenti, I. Jakoniuk, S.M. Anderson, B. Li, J. Pickel, R. Mckay, B. Nadal-Ginard, D.M. Bodine, A. Leri, P. Anversa, Bone marrow cells regenerate infarcted myocardium, Nature 410 (2001) 701–705.
[4] H. Oh, S.B. Bradfute, T.D. Gallardo, T. Nakamura, V. Gaussin, Y. Mishina, J. Pocius, L.H. Michael, R.R. Behringer, D.J. Garry, M.L. Entman, M.D. Schneider, Cardiac progenitor cells from adult myocardium: homing, differentiation, and fusion after infarction, Proc. Natl. Acad. Sci. USA 100 (2003) 12313–12318.
[5] D. Orlic, J. Kajstura, S. Chimenti, F. Limana, I. Jakoniuk, F. Quaini, B. Nadal-Ginard, D.M. Bodine, A. Leri, P. Anversa, Mobilized bone marrow cells repair the infarcted heart, improving function and survival, Proc. Natl. Acad. Sci. USA 98 (2001) 10344–10349.
[6] T. Asahara, T. Takahashi, H. Masuda, C. Kalka, D. Chen, H. Iwaguro, Y. Inai, M. Silver, J.M. Isner, VEGF contributes to postnatal neovascularization by mobilizing bone marrow-derived endothelial progenitor cells, EMBO J. 18 (1999) 3964–3972.
[7] T. Murata, T. Murai, T. Kanai, Y. Ogaki, K. Sanai, H. Kanda, S. Sato, N. Kajikawa, T. Umetsu, H. Matsuura, General pharmacology of beraprost sodium, Arzneimittelforschung 39 (1989) 867–876.
[8] T. Akiba, M. Miyazaki, N. Toda, Vasodilator actions of TRK-100, a new prostaglandin I2 analogue, Br. J. Pharmacol. 89 (1986) 703–711.
[9] S. Nishio, H. Matsuura, N. Kanai, Y. Fukatsu, T. Hirano, N. Nishikawa, K. Kameoka, T. Umetsu, The in vitro and ex vivo antiplatelet effect of TRK-100, a stable prostacyclin analog, in several species, Jpn J. Pharmacol. 47 (1988) 1–10.
[10] J.L. Demolis, A. Robert, M. Mouren, C. Funck-Brentano, P. Jaillon, Pharmacokinetics and platelet antiaggregating effects of beraprost, an oral stable prostacyclin analogue, in healthy volunteers, J. Cardiovasc. Pharmacol. 22 (1993) 711–716.
[11] P. Nony, P. Ffrench, P. Girard, S. Delair, S. Azoulay, J.P. Girre, M. Dechavanne, J.P. Boissel, Platelet-aggregation inhibition and hemodynamic effects of beraprost sodium, a new oral prostacyclin derivative: a study in healthy male subjects, Can. J. Physiol. Pharmacol. 74 (1996) 887–893.
[12] M. Murakami, M. Watanabe, H. Furukawa, H. Nakahara, The prostacyclin analogue beraprost sodium prevents occlusion of bypass grafts in patients with lower extremity arterial occlusive disease: a 20-year retrospective study, Ann. Vasc. Surg. 19 (2005) 838–842.
[13] L.T. Cooper, Beraprost for the treatment of intermittent claudication, J. Am. Coll. Cardiol. 41 (2003) 1679–1686.
[14] Y. Okano, T. Yoshioka, A. Shimouchi, T. Satoh, T. Kunieda, Orally active prostacyclin analogue in primary pulmonary hypertension, Lancet 349 (1997) 1365.

[15] N. Nagaya, M. Uematsu, Y. Okano, T. Satoh, S. Kyotani, F. Sakamaki, N. Nakanishi, K. Miyatake, T. Kunieda, Effect of orally active prostacyclin analogue on survival of outpatients with primary pulmonary hypertension, J. Am. Coll. Cardiol. 34 (1999) 1188–1192.
[16] A.M. Lefer, M.L. Ogletree, J.B. Smith, M.J. Silver, K.C. Nicolaou, W.E. Barnette, G.P. Gasic, Prostacyclin: a potentially valuable agent for preserving myocardial tissue in acute myocardial ischemia, Science 200 (1978) 52–54.
[17] B.I. Jugdutt, G.M. Hutchins, B.H. Bulkley, L.C. Becker, Dissimilar effects of prostacyclin, prostaglandin E1, and prostaglandin E2 on myocardial infarct size after coronary occlusion in conscious dogs, Circ. Res. 49 (1981) 685–700.
[18] J.A. Melin, L.C. Becker, Salvage of ischemic myocardium by prostacyclin during experimental myocardial infarction, J. Am. Coll. Cardiol. 2 (1983) 279–286.
[19] K. Niwano, M. Arai, K. Tomaru, T. Uchiyama, Y. Ohyama, M. Kurabayashi, Transcriptional stimulation of the eNOS gene by the stable prostacyclin analogue beraprost is mediated through cAMP-responsive element in vascular endothelial cells: close link between PGI2 signal and NO pathways, Circ. Res. 93 (2003) 523–530.
[20] A. Aicher, C. Heeschen, C. Mildner-Rihm, C. Urbich, C. Ihling, K. Technau-Ihling, A.M. Zeiher, S. Dimmeler, Essential role of endothelial nitric oxide synthase for mobilization of stem and progenitor cells, Nat. Med. 9 (2003) 1370–1376.
[21] T. Nishikimi, K. Uchino, E.D. Frohlich, Effects of α1-adrenergic blockade on intrarenal hemodynamics in heart failure rats, Am. J. Physiol. Regul. Integr. Comp. Physiol. 262 (1998) R198–R203.
[22] P.S. Douglas, N. Reichek, T. Plappert, A. Muhammad, M.G. St John Sutton, Comparison of echocardiographic methods for assessment of left ventricular shortening and wall stress, J. Am. Coll. Cardiol. 9 (1987) 945–951.
[23] Y.W. Chien, R.W. Barbee, A.A. Macphee, E.D. Frohlich, N.C. Trippondo, Increased ANF secretion after volume expansion is preserved in rats with heart failure, Am. J. Physiol. 254 (1988) R185–R191.
[24] T. Ito, A. Suzuki, E. Imai, M. Okabe, M. Hori, Bone marrow is a reservoir of repopulating mesangial cells during glomerular remodeling, J. Am. Soc. Nephrol. 12 (2001) 2625–2635.
[25] P.J. Simpson, R.F. Todd 3rd, J.C. Fantone, J.K. Mickelson, J.D. Griffin, B.R. Lucchesi, Reduction of experimental canine myocardial reperfusion injury by a monoclonal antibody (anti-Mo1, anti-CD11b) that inhibits leukocyte adhesion, J. Clin. Invest. 81 (1988) 624–629.
[26] W.W. Nichols, J. Mehta, T.J. Wargovich, D. Franzini, D. Lawson, Reduced myocardial neutrophil accumulation and infarct size following thromboxane synthetase inhibitor or receptor antagonist, Angiology 40 (1989) 209–221.
[27] M. Kainoh, R. Imai, T. Nakadake, M. Hattori, S. Nishio, Prostacyclin and beraprost sodium as suppressors of activated rat polymorphonuclear leukocytes, Biochem. Pharmacol. 39 (1990) 477–483.
[28] Y. Ueno, Y. Miyauchi, S. Nishio, Beraprost sodium protects occlusion/reperfusion injury in the dog by inhibition of neutrophil migration, Gen. Pharmacol. 25 (1994) 427–432.
[29] A. Kawamoto, T. Tkebuchava, J. Yamaguchi, H. Nishimura, Y.S. Yoon, C. Milliken, S. Uchida, O. Masuo, H. Iwaguro, H. Ma, A. Hanley, M. Silver, M. Iearney, D.W. Losordo, J.M. Isner, T. Asahara, Intramyocardial transplantation of autologous endothelial progenitor cells for therapeutic neovascularization of myocardial ischemia, Circulation 107 (2003) 461–468.
[30] A. Kawamoto, T. Asahara, D.W. Losordo, Transplantation of endothelial progenitor cells for therapeutic neovascularization, Cardiovasc. Radiat. Med. 3 (2002) 221–225.
[31] A. Weber, I. Pedrosa, A. Kawamoto, N. Himes, J. Munasinghe, T. Asahara, N.M. Rofsky, D.W. Losordo, Magnetic resonance mapping of transplanted endothelial progenitor cells for therapeutic neovascularization in ischemic heart disease, Eur. J. Cardiothorac. Surg. 26 (2004) 137–143.
[32] J. Kajstura, M. Rota, B. Whang, S. Cascapera, T. Hosoda, C. Bearzi, D. Nurzynska, H. Kasahara, E. Zias, M. Bonafe, B. Nadal-Ginard, D. Torella, A. Nascimbene, F. Quaini, K. Urbanek, A. Leri, P. Anversa, Bone marrow cells differentiate in cardiac cell lineages after infarction independently of cell fusion, Circ. Res. 96 (2005) 127–137.
[33] R. Lanza, M.A. Moore, T. Wakayama, A.C. Perry, J.H. Shieh, J. Hendrikx, A. Leri, S. Chimenti, A. Monsen, D. Nurzynska, M.D. West, J. Kajstura, P. Anversa, Regeneration of the infarcted heart with stem cells derived by nuclear transplantation, Circ. Res. 94 (2004) 820–827.
[34] Y. Uchida, T. Hanai, K. Hasegawa, K. Kawamura, T. Oshima, Recanalization of obstructed coronary artery by intracoronary administration of prostacyclin in patients with acute myocardial infarction, Adv. Prostaglandin Thromboxane Leukot. Res. 11 (1983) 377–383.
[35] C.Y. Xiao, A. Hara, Yuhki K, T. Fujino, H. Ma, Y. Okada, O. Takahata, T. Yamada, T. Murata, S. Narumiya, F. Ushikubi, Roles of prostaglandin I(2) and thromboxane A(2) in cardiac ischemia–reperfusion injury: a study using mice lacking their respective receptors, Circulation 104 (2001) 2210–2215.
[36] A. Szczeklik, J. Szczeklik, R. Nizankowski, P. Gluszko, Prostacyclin for unstable angina, N. Engl. J. Med. 303 (1980) 881.
[37] M.L. Knudtson, V.F. Flintoft, D.L. Roth, J.L. Hansen, H.J. Duff, Effect of short-term prostacyclin administration on restenosis after percutaneous transluminal coronary angioplasty, J. Am. Coll. Cardiol. 15 (1990) 691–697.
[38] F. Kuethe, H.R. Figulla, M. Herzau, M. Voth, M. Fritzenwanger, T. Opfermann, K. Pachmann, A. Krack, H.G. Sayer, D. Gottschild, G.S. Werner, Treatment with granulocyte colony-stimulating factor for mobilization of bone marrow cells in patients with acute myocardial infarction, Am. Heart J. 150 (2005) 115.
[39] H.J. Kang, H.S. Kim, S.Y. Zhang, K.W. Park, H.J. Cho, B.K. Koo, Y.J. Kim, D. Soo Lee, D.W. Sohn, K.S. Han, B.H. Oh, M.M. Lee, Y.B. Park, Effects of intracoronary infusion of peripheral blood stem-cells mobilised with granulocyte-colony stimulating factor on left ventricular systolic function and restenosis after coronary stenting in myocardial infarction: the MAGIC cell randomised clinical trial, Lancet 363 (2004) 751–756.
[40] R.M. Califf, K.F. Adams, W.J. McKenna, M. Gheorghiade, B.F. Uretsky, S.E. McNulty, H. Darius, K. Schulman, F. Zannad, E. Handberg-Thurmond, F.E. Harrell Jr., W. Wheeler, J. Soler-Soler, K. Swedberg, A randomized controlled trial of epoprostenol therapy for severe congestive heart failure: The Flolan International Randomized Survival Trial (FIRST), Am. Heart J. 134 (1997) 44–54.
[41] M. Lievre, S. Morand, B. Besse, J.N. Fiessinger, J.P. Boissel, Oral beraprost sodium, a prostaglandin I(2) analogue, for intermittent claudication: a double-blind, randomized, multicenter controlled trial. Beraprost et Claudication Intermittente (BERCI) Research Group, Circulation 102 (2000) 426–431.
[42] E.R. Mohler 3rd, W.R. Hiatt, J.W. Olin, M. Wade, R. Jeffs, A.T. Hirsch, Treatment of intermittent claudication with beraprost sodium, an orally active prostaglandin I2 analogue: a double-blinded, randomized, controlled trial, J. Am. Coll. Cardiol. 41 (2003) 1679–1686.

Japanese Journal of Applied Physics
Vol. 45, No. 6A, 2006, pp. 5301–5306

X-ray Spectra from Weakly Ionized Linear Copper Plasma

Eiichi SATO, Yasuomi HAYASHI, Rudolf GERMER[1], Etsuro TANAKA[2], Hidezo MORI[3], Toshiaki KAWAI[4], Takashi INOUE[5], Akira OGAWA[5], Shigehiro SATO[6], Kazuyoshi TAKAYAMA[7] and Jun ONAGAWA[8]

Department of Physics, Iwate Medical University, 3-16-1 Honchodori, Morioka 020-0015, Japan
[1]*ITP, FHTW FB1 and TU-Berlin, Blankenhainer Str. 9, D 12249 Berlin, Germany*
[2]*Department of Nutritional Science, Faculty of Applied Bio-science, Tokyo University of Agriculture, 1-1-1 Sakuragaoka, Setagaya-ku, Tokyo 156-8502, Japan*
[3]*Department of Cardiac Physiology, National Cardiovascular Center Research Institute, 5-7-1 Fujishirodai, Suita, Osaka 565-8565, Japan*
[4]*Electron Tube Division #2, Hamamatsu Photonics K.K., 314-5 Shimokanzo, Iwata, Shizuoka 438-0193, Japan*
[5]*Department of Neurosurgery, School of Medicine, Iwate Medical University, 19-1 Uchimaru, Morioka 020-8505, Japan*
[6]*Department of Microbiology, School of Medicine, Iwate Medical University, 19-1 Uchimaru, Morioka 020-8505, Japan*
[7]*Shock Wave Research Center, Institute of Fluid Science, Tohoku University, 2-1-1 Katahira, Sendai 980-8577, Japan*
[8]*Department of Applied Physics and Informatics, Faculty of Engineering, Tohoku Gakuin University, 1-13-1 Chuo, Tagajo, Miyagi 985-8537, Japan*

(Received November 20, 2005; accepted April 5, 2006; published online June 8, 2006)

In the plasma flash X-ray generator, a 200 nF condenser is charged up to 50 kV by a power supply, and flash X-rays are produced by the discharging. The X-ray tube is a demountable triode with a trigger electrode, and the turbomolecular pump evacuates air from the tube with a pressure of approximately 1 mPa. Target evaporation leads to the formation of weakly ionized linear plasma, consisting of copper ions and electrons, around the fine target, and intense Kα lines are left using a 10-μm-thick nickel filter. At a charging voltage of 50 kV, the maximum tube voltage was almost equal to the charging voltage of the main condenser, and the peak current was about 16 kA. The K-series characteristic X-rays were clean and intense, and higher harmonic X-rays were observed. The X-ray pulse widths were approximately 300 ns, and the time-integrated X-ray intensity had a value of approximately 1.5 mGy per pulse at 1.0 m from the X-ray source with a charging voltage of 50 kV. [DOI: 10.1143/JJAP.45.5301]

KEYWORDS: linear plasma, X-ray spectra, K-series characteristic X-rays, bremsstrahlung X-rays, higher harmonic X-rays

1. Introduction

In order to produce X-ray lasers, several different methods have been developed, and a discharge capillary[1–3] is very useful to increase the laser pulse energy with increases in the capillary length. However, it is difficult to increase the laser photon energy to 10 keV or beyond.

Using monochrocollimators, synchrotrons produce monochromatic parallel beams, which are fairly similar to monochromatic parallel laser beams, and the beams have been applied to various research project including phase-contrast radiography[4,5] and enhanced K-edge angiography.[6,7] Because there are no X-ray resonators in the high-photon-energy region, new methods for increasing coherence will be desired in the future.

To apply flash X-ray generators to biomedicine, several different generators[8–13] have been developed, and plasma X-ray generators[14–17] are useful for producing clean characteristic X-rays in the low-photon-energy region of less than 10 keV. By forming weakly ionized linear plasma using rod targets, intense K-series characteristic X-rays are observed from the axial direction of the linear plasmas of nickel and copper, since the bremsstrahlung X-rays are absorbed effectively by the linear plasma. We are therefore very interested in the X-ray spectra produced by increasing the charging voltage in the high photon energy region beyond Kβ energies.

In this paper, we describe a recent table-top plasma flash X-ray generator utilizing a rod target triode, used to perform a preliminary experiment for generating clean K-series characteristic X-rays and their higher harmonic hard X-rays by forming a linear copper plasma cloud around a fine target.

2. Generator

Figure 1 shows a block diagram of the high-intensity plasma flash X-ray generator. This generator consists of the following essential components: a high-voltage power supply, a high-voltage condenser with a capacity of approximately 200 nF, a turbomolecular pump, a krytron pulse generator as a trigger device, and a flash X-ray tube. The high-voltage main condenser is charged to 50 kV by the power supply, and electric charges in the condenser are discharged to the tube after triggering the cathode electrode with the trigger device. The plasma flash X-rays are then produced.

The X-ray tube is a demountable cold-cathode triode that is connected to the turbomolecular pump with a pressure of approximately 1 mPa. This tube consists of the following major parts: a hollow cylindrical carbon cathode with a bore diameter of 10.0 mm, a brass focusing electrode, a trigger electrode made from copper wire, a stainless steel vacuum chamber, a nylon insulator, a poly(ethylene terephthalate) (Mylar) X-ray window 0.25 mm in thickness, and a rod-shaped copper target 3.0 mm in diameter with a tip angle of 60°. The distance between the target and cathode electrodes is approximately 20 mm, and the trigger electrode is set in the cathode electrode. As electron beams from the cathode electrode are roughly converged to the target by the focusing electrode, evaporation leads to the formation of a weakly ionized linear plasma,[18] consisting of copper ions and electrons, around the fine target.

In the linear plasma, bremsstrahlung photons with energies higher than the K-absorption edge are effectively absorbed and are converted into fluorescent X-rays. The plasma then transmits the fluorescent rays easily, and bremsstrahlung rays with energies lower than the K-edge

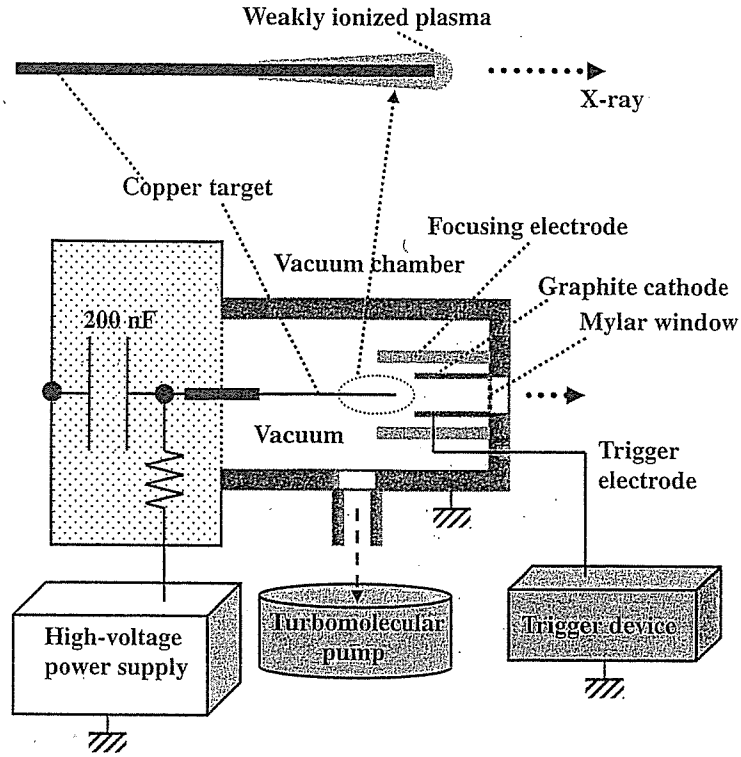

Fig. 1. Block diagram including the electric circuit of the plasma flash X-ray generator.

are also absorbed by the plasma. In addition, because bremsstrahlung rays are not emitted in the opposite direction to that of electron trajectory, intense characteristic X-rays are generated from the plasma-axial direction.

3. Characteristics

3.1 Tube voltage and current

Tube voltage and current were measured by a high-voltage divider with an input impedance of 1 GΩ and a current transformer, respectively. The withstand voltage of the divider is approximately 60 kV, and the measurable current of the transformer ranges from 1 A to 100 kA. Figure 2 shows the time relation between the tube voltage and current. At the indicated charging voltages, they roughly displayed damped oscillations. When the charging voltage was increased, both the maximum tube voltage and current increased. At a charging voltage of 50 kV, the maximum tube voltage was almost equal to the charging voltage of the main condenser, and the maximum tube current was approximately 16 kA.

3.2 X-ray output

X-ray output pulse was detected using a combination of a plastic scintillator and a photomultiplier (Fig. 3). The X-ray pulse height substantially increased with corresponding increases in the charging voltage. The rise time increased with increasing the voltage because the K-series characteristic X-rays were produced with tube voltages beyond the critical excitation voltage of 8.9 kV. The X-ray pulse widths were about 300 ns, and the time-integrated X-ray intensity per pulse measured by a thermoluminescence dosimeter (Kyokko TLD Reader 1500 having MSO-S elements without energy compensation) had a value of approximately 1.5 mGy at 1.0 m from the X-ray source with a charging voltage of 50 kV. The TLD reader has a wide measurable range of from 1 μSv to 100 Sv.

3.3 X-ray source

In order to roughly observe images of the plasma X-ray source in the detector plane, we employed a pinhole camera with a hole diameter of 100 μm without using a filter (Fig. 4). When the charging voltage was increased, the plasma X-ray source grew, and both spot dimension and intensity increased. Because the X-ray intensity is the highest at the center of the spot, both the dimension and intensity decreased according to both increases in the thickness of a filter for absorbing X-rays and decreases in the pinhole diameter.

3.4 X-ray spectra

X-ray spectra from the plasma source were measured by a transmission-type spectrometer with a lithium fluoride curved crystal 0.5 mm in thickness. The spectra were taken by a computed radiography (CR) system[19] (Konica Minolta, Regius 150) with a wide dynamic range beyond five figures for measuring X-ray intensity, and relative X-ray intensity was calculated from Dicom digital data. Subsequently, the relative X-ray intensity as a function of the data was calibrated using a conventional X-ray generator, and we confirmed that the intensity was proportional to the exposure time. Figure 5 shows measured spectra from the copper target at the indicated conditions. In fact, we observed clean K lines, and Kα lines were left by absorbing Kβ lines using a 10-μm-thick nickel filter. When the charging voltage was increased, the characteristic X-ray intensity substantially increased. In particular, we confirmed the irradiation of

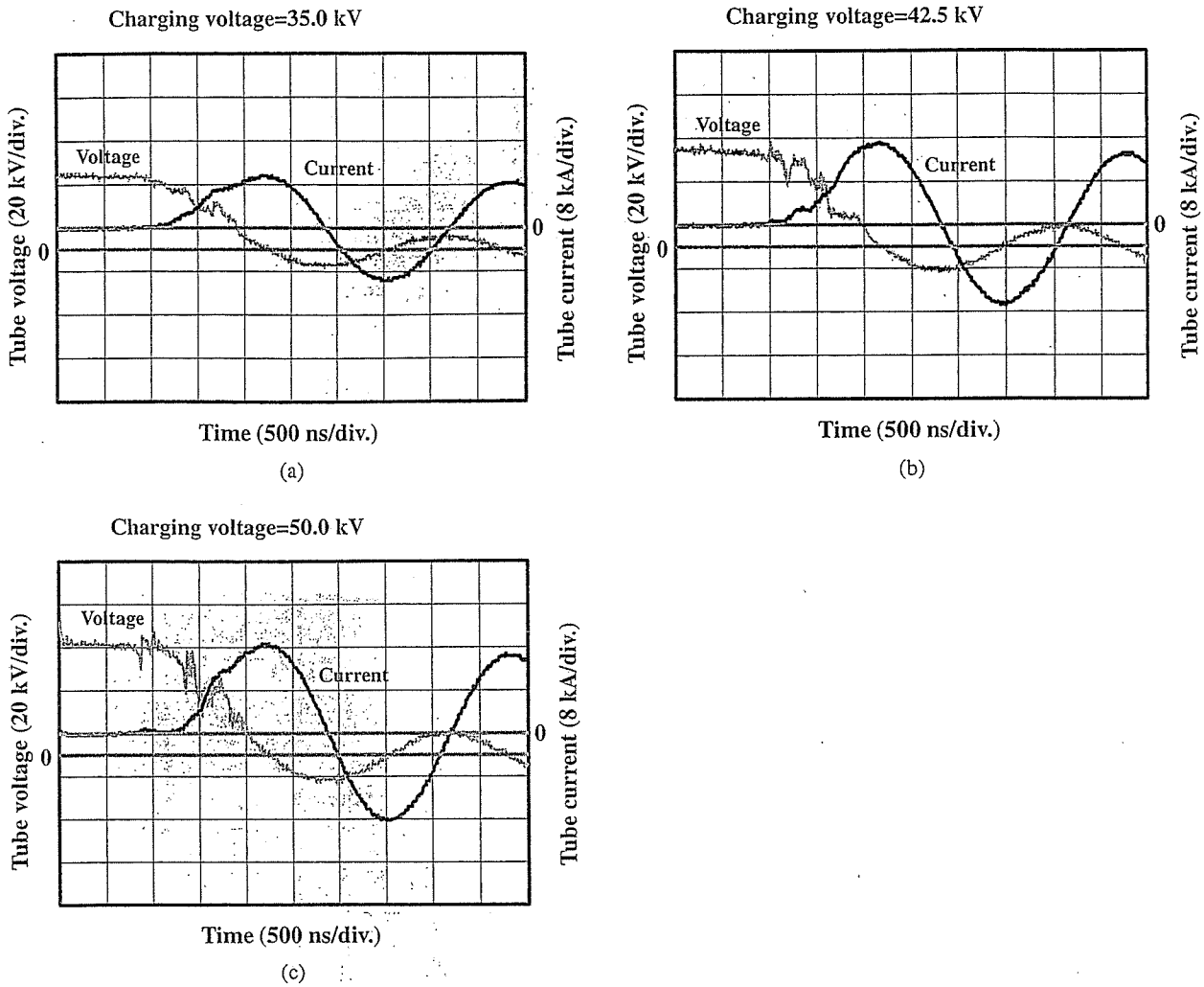

Fig. 2. Tube voltages and currents with a charging voltage of (a) 35.0, (b) 42.5, and (b) 50.0 kV.

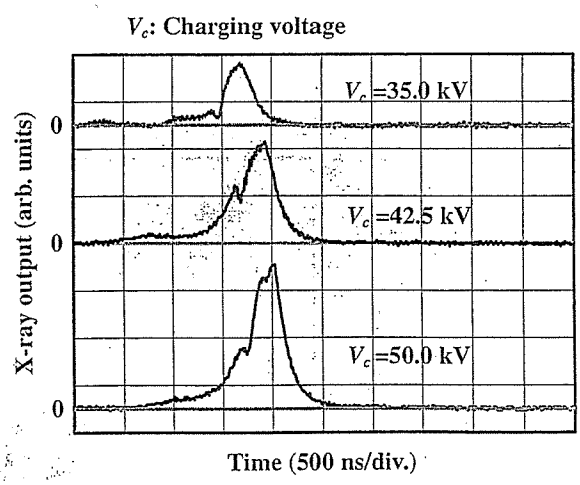

Fig. 3. X-ray outputs at the indicated conditions.

the second and fourth harmonic X-rays of the fundamental K-series characteristic X-rays from copper target. The X-ray intensities of the harmonics increased with increases in the charging voltage, and the harmonic bremsstrahlung rays survived due to the X-ray resonation in the plasma.

4. Radiography

The plasma radiography was performed by the CR system using the filter. The charging voltage and the distance between the X-ray source and imaging plate were 50 kV and 1.2 m, respectively. First, rough measurements of spatial resolution were made using wires. Figure 6 shows radiograms of tungsten wires coiled around pipes made of poly(methyl methacrylate) (PMMA). Although the image contrast decreased somewhat with decreases in the wire diameter, due to blurring of the image caused by the sampling pitch of 87.5 μm, a 50-μm-diameter wire could be observed.

Figure 7 shows a radiogram of plastic bullets falling into a polypropylene beaker from a plastic test tube. Because the X-ray duration was about 0.5 μs, the stop-motion image of bullets could be obtained. Next, a radiogram of a vertebra is shown in Fig. 8, and fine structures in the vertebra were observed. Finally, Fig. 9 shows an angiogram of a rabbit ear; iodine-based microspheres of 15 μm in diameter were used, and fine blood vessels of about 100 μm were visible.

5. Conclusions and Outlook

We obtained fairly intense and clean K lines from a weakly ionized linear copper plasma, and Kα lines were left

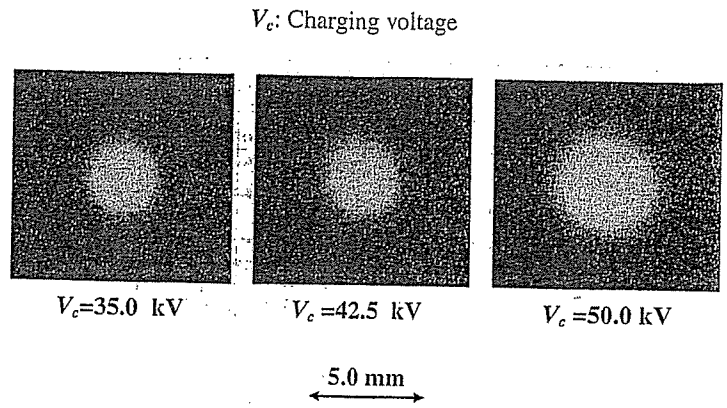

Fig. 4. Images of the plasma X-ray source.

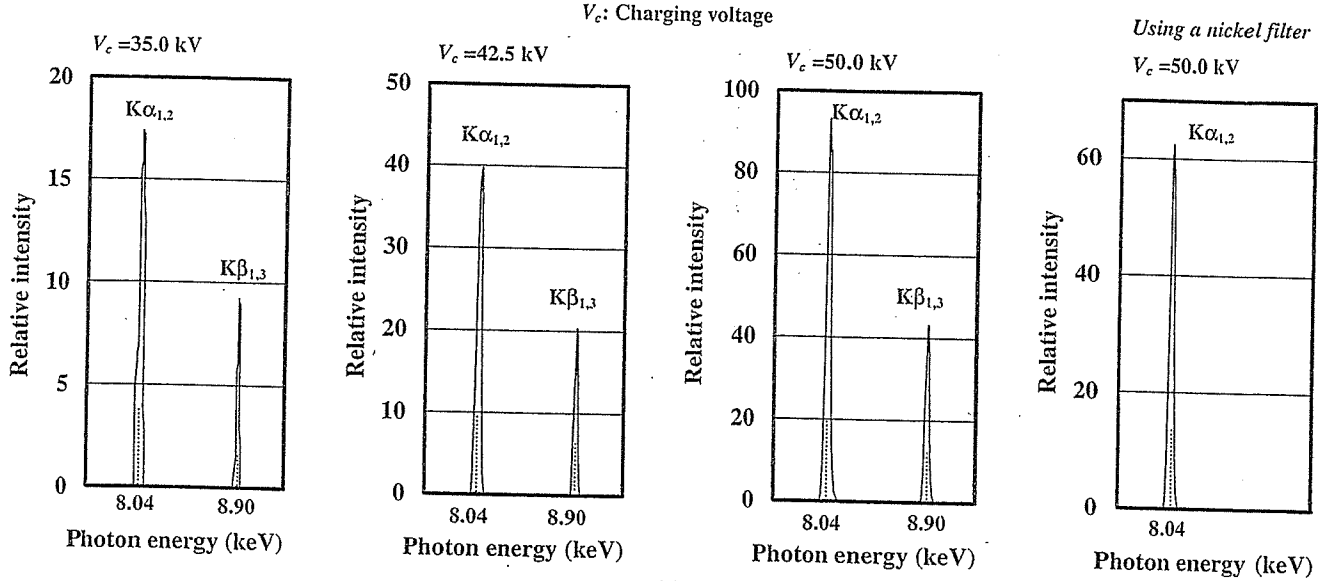

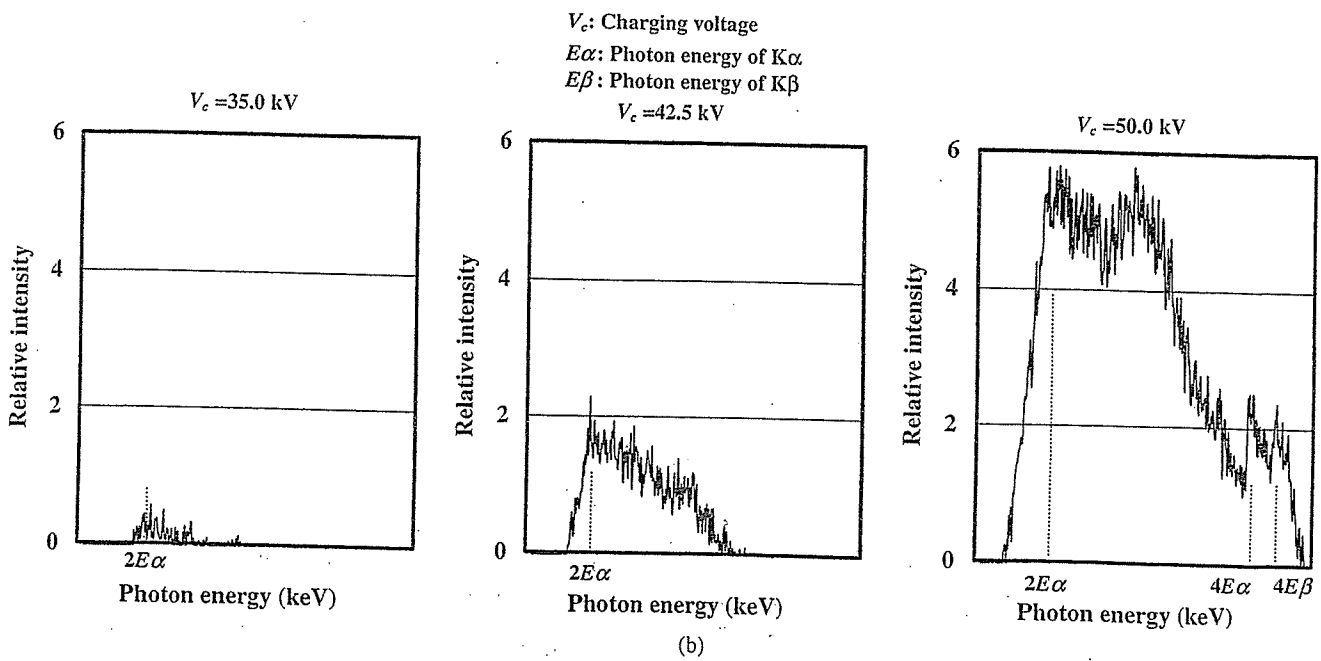

Fig. 5. X-ray spectra from weakly ionized copper plasma at the indicated conditions. (a) characteristic X-rays and (b) higher harmonic X-rays.

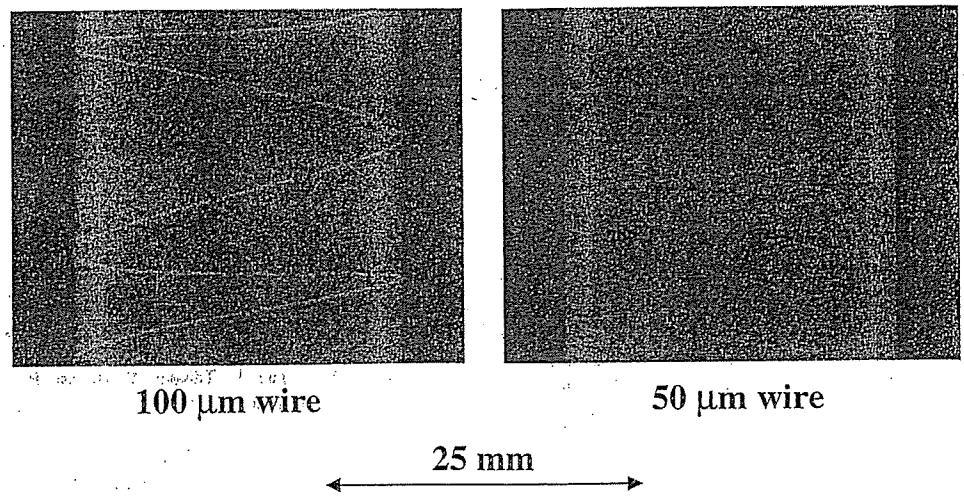

Fig. 6. Radiograms of tungsten wires coiled around PMMA pipes.

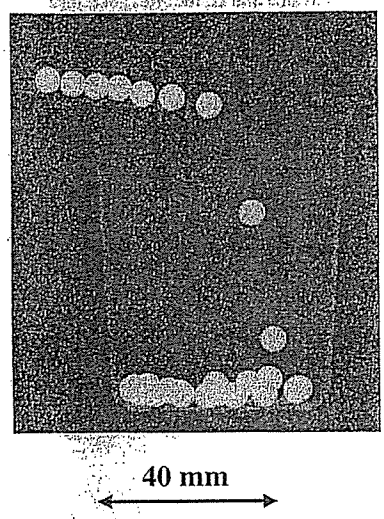

Fig. 7. Radiogram of plastic bullets falling into polypropylene beaker from a plastic test tube.

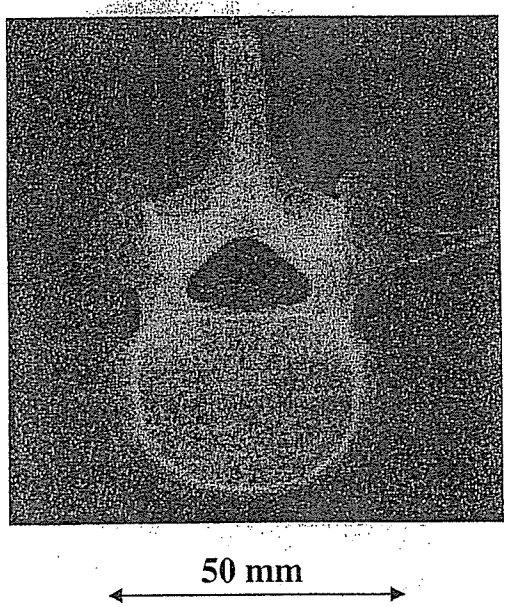

Fig. 8. Radiogram of a vertebra.

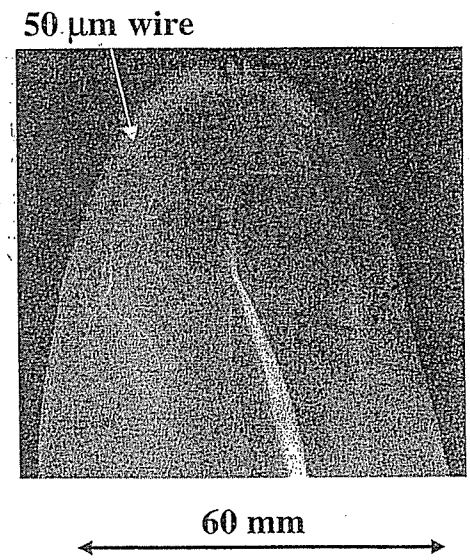

Fig. 9. Angiogram of a rabbit ear.

by the nickel filter. Both the characteristic and the harmonic X-ray intensities substantially increased with increasing the charging voltage.

In cases where weakly ionized linear plasma is employed, intense and clean K-series characteristic X-rays can be obtained. However, it is not easy to produce high-photon-energy K-series characteristic X-rays because the linear plasma transmits high-photon-energy bremsstrahlung X-rays; the effective thickness of a monochromatic metal filter increases with increases in the atomic number. Therefore, high-photon-energy plasma flash X-ray generators utilizing the angle dependence of bremsstrahlung X-rays are very useful to produce K photons of molybdenum, silver, cerium, tantalum, and tungsten. In particular, Kα rays of tantalum and tungsten are useful for performing enhanced K-edge angiography using gadolinium contrast media, and cerium K rays can be employed to perform iodine K-edge angiography.

In this research, we obtained sufficient characteristic X-ray intensity per pulse for CR radiography, and the

generator produced number of characteristic K photons was approximately 1×10^8 photons/cm^2 at 1.0 m per pulse. In addition, we are very interested in producing steady-state clean K rays and their higher harmonic hard X-rays using a similar tube.

Acknowledgments

This work was supported by Grants-in-Aid for Scientific Research (13470154, 13877114, 16591181, and 16591222) and Advanced Medical Scientific Research from MECSST, Health and Labor Sciences Research Grants (RAMT-nano-001, RHGTEFB-genome-005 and RHGTEFB-saisei-003), Grants from The Keiryo Research Foundation, The Promotion and Mutual Aid Corporation for Private Schools of Japan, Japan Science and Technology Agency (JST), and the New Energy and Industrial Technology Development Organization (NEDO, Industrial Technology Research Grant Program in '03).

1) J. J. Rocca, V. Shlyaptsev, F. G. Tomasel, O. D. Cortazar, D. Hartshorn and J. L. A. Chilla: Phys. Rev. Lett. **73** (1994) 2192.
2) C. D. Macchietto, B. R. Benware and J. J. Rocca: Opt. Lett. **24** (1999) 1115.
3) J. J. G. Rocca, J. L. A. Chilla, S. Sakadzic, A. Rahman, J. Filevich, E. Jankowska, E. C. Hammarsten, B. M. Luther, H. C. Kapteyn, M. Murnane and V. N. Shlyapsev: Proc. SPIE **4505** (2001) 1.
4) A. Momose, T. Takeda, Y. Itai and K. Hirano: Nat. Med. **2** (1996) 473.
5) M. Ando, A. Maksimenko, H. Sugiyama, W. Pattanasiriwisawa, K. Hyodo and C. Uyama: Jpn. J. Appl. Phys. **41** (2002) L1016.
6) H. Mori *et al.*: Radiology **201** (1996) 173.
7) K. Hyodo, M. Ando, Y. Oku, S. Yamamoto, T. Takeda, Y. Itai, S. Ohtsuka, Y. Sugishita and J. Tada: J. Synchrotron Radiat. **5** (1998) 1123.
8) E. Sato, S. Kimura, S. Kawasaki, H. Isobe, K. Takahashi, Y. Tamakawa and T. Yanagisawa: Rev. Sci. Instrum. **61** (1990) 2343.
9) K. Takahashi, E. Sato, M. Sagae, T. Oizumi, Y. Tamakawa and T. Yanagisawa: Jpn. J. Appl. Phys. **33** (1994) 4146.
10) E. Sato, K. Takahashi, M. Sagae, S. Kimura, T. Oizumi, Y. Hayasi, Y. Tamakawa and T. Yanagisawa: Med. Biol. Eng. Comput. **32** (1994) 289.
11) E. Sato, M. Sagae, K. Takahashi, A. Shikoda, T. Oizumi, Y. Hayasi, Y. Tamakawa and T. Yanagisawa: Med. Biol. Eng. Comput. **32** (1994) 295.
12) E. Sato, M. Sagae, E. Tanaka, Y. Hayasi, R. Germer, H. Mori, T. Kawai, T. Ichimaru, S. Sato, K. Takayama and H. Ido: Jpn. J. Appl. Phys. **43** (2004) 7324.
13) E. Sato, E. Tanaka, H. Mori, T. Kawai, T. Ichimaru, S. Sato, K. Takayama and H. Ido: Med. Phys. **32** (2005) 49.
14) E. Sato, Y. Hayasi, R. Germer, E. Tanaka, H. Mori, T. Kawai, H. Obara, T. Ichimaru, K. Takayama and H. Ido: Jpn. J. Med. Phys. **23** (2003) 123.
15) E. Sato, Y. Hayasi, R. Germer, E. Tanaka, H. Mori, T. Kawai, T. Ichimaru, K. Takayama and H. Ido: Rev. Sci. Instrum. **74** (2003) 5236.
16) E. Sato, Y. Hayasi, R. Germer, E. Tanaka, H. Mori, T. Kawai, T. Ichimaru, S. Sato, K. Takayama and H. Ido: J. Electron Spectrosc. Relat. Phenom. C **137–140** (2004) 713.
17) E. Sato, E. Tanaka, H. Mori, T. Kawai, S. Sato and K. Takayama: Opt. Eng. **44** (2005) 049002.
18) E. Sato, M. Sagae, K. Takahashi, T. Ichimaru, W. Aiba, S. Kumagai, Y. Hayasi, H. Ido, K. Sakamaki, K. Takayama and Y. Tamakawa: Proc. SPIE **3336** (1998) 75.
19) E. Sato, K. Sato and Y. Tamakawa: Ann. Rep. Iwate Med. Univ. Sch. Lib. Arts Sci. **35** (2000) 13.

Available online at www.sciencedirect.com
ScienceDirect
Radiation Physics and Chemistry 75 (2006) 1812–1818
Radiation Physics and Chemistry
www.elsevier.com/locate/radphyschem

Preliminary study for producing higher harmonic hard X-rays from weakly ionized nickel plasma

Eiichi Sato[a,*], Yasuomi Hayasi[a], Etsuro Tanaka[b], Hidezo Mori[c], Toshiaki Kawai[d], Takashi Inoue[e], Akira Ogawa[e], Shigehiro Sato[f], Kazuyoshi Takayama[g], Jun Onagawa[h], Hideaki Ido[h]

[a]*Department of Physics, Iwate Medical University, 3-16-1 Honchodori, Morioka 020-0015, Japan*
[b]*Department of Nutritional Science, Faculty of Applied Bio-science, Tokyo University of Agriculture, 1-1-1 Sakuragaoka, Setagaya-ku 156-8502, Japan*
[c]*Department of Cardiac Physiology, National Cardiovascular Center Research Institute, 5-7-1 Fujishirodai, Suita, Osaka 565-8565, Japan*
[d]*Electron Tube Division #2, Hamamatsu Photonics K. K., 314-5 Shimokanzo, Iwata 438-0193, Japan*
[e]*Department of Neurosurgery, School of Medicine, Iwate Medical Universichimaru, Morioka 020-8505, Japan*
[f]*Department of Microbiology, School of Medicine, Iwate Medical University, 19-1 Uchimaru, Morioka 020-8505, Japan*
[g]*Shock Wave Research Center, Institute of Fluid Science, Tohoku University, 2-1-1 Katahira, Sendai 980-8577, Japan*
[h]*Department of Applied Physics and Informatics, Faculty of Engineering, Tohoku Gakuin University, 1-13-1 Chuo, Tagajo 985-8537, Japan*

Accepted 23 November 2005

Abstract

In the plasma flash X-ray generator, a 200 nF condenser is charged up to 50 kV by a power supply, and flash X-rays are produced by the discharging. The X-ray tube is a demountable triode with a trigger electrode, and the turbomolecular pump evacuates air from the tube with a pressure of approximately 1 mPa. Target evaporation leads to the formation of weakly ionized linear plasma, consisting of nickel ions and electrons, around the fine target, and intense Kα lines are left using a 15-μm-thick cobalt filter. At a charging voltage of 50 kV, the maximum tube voltage was almost equal to the charging voltage of the main condenser, and the peak current was about 18 kA. The K-series characteristic X-rays were clean and intense, and higher harmonic X-rays were observed. The X-ray pulse widths were approximately 300 ns, and the time-integrated X-ray intensity had a value of approximately 1.0 mGy at 1.0 m from the X-ray source with a charging voltage of 50 kV.

PACS: 52.80.Vp; 52.90.+z; 87.59.Bh; 87.64.Gb

Keywords: Weakly ionized linear plasma; K-series characteristic X-rays; Clean characteristic X-rays; Higher harmonic hard X-rays

1. Introduction

In conjunction with single crystals, synchrotrons produce monochromatic parallel beams, which are fairly similar to monochromatic parallel laser beams, and the

*Corresponding author.
E-mail address: dresato@iwate-med.ac.jp (E. Sato).

0969-806X/$ - see front matter © 2006 Elsevier Ltd. All rights reserved.
doi:10.1016/j.radphyschem.2005.11.012

beams have been applied to enhanced K-edge angiography (Thompson et al., 1992; Mori et al., 1996; Hyodo et al., 1998), phase-contrast radiography (Davis et al., 1995; Momose et al., 1996; Ando et al., 2002), and crystallography. Therefore, the production of coherent hard X-ray lasers for various research projects, including biomedical applications, has long been wished for.

Recently, soft X-ray lasers have been produced by a gas-discharge capillary (Rocca et al., 1994, 1996; Macchietto et al., 1999), and the laser pulse energy substantially increased in proportion to the capillary length. These kinds of fast discharges can generate hot and dense plasma columns with aspect ratios approaching 1000:1. However, it is difficult to increase the laser photon energy to 10 keV or beyond. Because there are no X-ray resonators in the high-photon-energy region, new methods for increasing coherence will be desired in the future.

To apply flash X-ray generators to biomedicine, several different generators have been developed (Germer, 1979; Sato et al., 1990, 1994a, b; Shikoda et al., 1994; Takahashi et al., 1994), and plasma X-ray generators (Sato et al., 2003a, b, 2004a–c, 2005a–c) are useful for producing clean characteristic X-rays in the low-photon-energy region of less than 20 keV. By forming weakly ionized linear plasma using rod targets, we confirmed irradiation of intense K-series characteristic X-rays from the axial direction of the linear plasmas of nickel, copper, and molybdenum, since the bremsstrahlung X-rays are absorbed effectively by the linear plasma; monochromatic clean Kα rays were produced using K-edge filters.

In this paper, we describe a recent plasma flash X-ray generator utilizing a rod target, used to perform a preliminary experiment for generating clean K-series characteristic X-rays and their higher harmonic hard X-rays by forming a plasma cloud around a fine target.

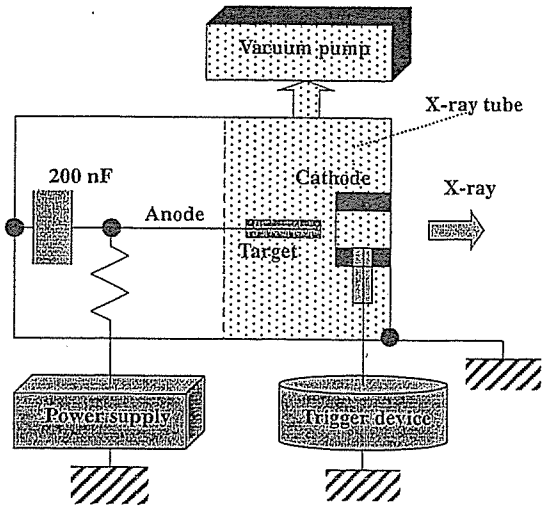

Fig. 1. Block diagram including electric circuit of the plasma flash X-ray generator.

2. Generator

Fig. 1 shows a block diagram of the high-intensity plasma flash X-ray generator. This generator consists of the following essential components: a high-voltage power supply, a high-voltage condenser with a capacity of approximately 200 nF, a turbomolecular pump, a krytron pulse generator as a trigger device, and a flash X-ray tube. The high-voltage main condenser is charged to 50 kV by the power supply, and electric charges in the condenser are discharged to the tube after triggering the cathode electrode with the trigger device. The plasma flash X-rays are then produced.

The schematic drawing of the plasma X-ray tube is illustrated in Fig. 2. The X-ray tube is a demountable

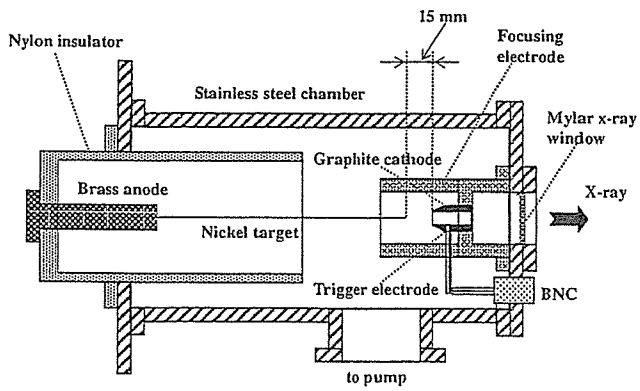

Fig. 2. Schematic drawing of the flash X-ray tube with a rod nickel target.

cold-cathode triode that is connected to the turbomolecular pump with a pressure of approximately 1 mPa. This tube consists of the following major parts: a hollow cylindrical carbon cathode with a bore diameter of 10.0 mm, a brass focusing electrode, a trigger electrode made from copper wire, a stainless steel vacuum chamber, a nylon insulator, a polyethylene terephthalate (Mylar) X-ray window 0.25 mm in thickness, and a rod-shaped nickel target 3.0 mm in diameter with a tip angle of 60°. The distance between the target and cathode electrodes is approximately 15 mm, and the trigger electrode is set in the cathode electrode. As electron beams from the cathode electrode are roughly converged to the target by the focusing electrode, evaporation leads to the formation of a weakly ionized linear plasma, consisting of nickel ions and electrons, around the fine target.

In the linear plasma, bremsstrahlung photons with energies higher than the K-absorption edge are effectively absorbed and are converted into fluorescent X-rays. The plasma then transmits the fluorescent rays easily, and bremsstrahlung rays with energies lower than the K-edge are also absorbed by the plasma. In addition, because bremsstrahlung rays are not emitted in the opposite direction to that of electron trajectory, intense characteristic X-rays are generated from the plasma-axial direction.

3. Characteristics

3.1. Tube voltage and current

Tube voltage and current were measured by a high-voltage divider with an input impedance of 1 GΩ and a current transformer, respectively. Fig. 3 shows the time relation between the tube voltage and current. At the indicated charging voltages, they roughly displayed damped oscillations. When the charging voltage was increased, both the maximum tube voltage and current increased. At a charging voltage of 50 kV, the maximum tube voltage was almost equal to the charging voltage of the main condenser, and the maximum tube current was approximately 18 kA.

3.2. X-ray output

X-ray output pulse was detected using a combination of a plastic scintillator and a photomultiplier (Fig. 4). The X-ray pulse height substantially increased with corresponding increases in the charging voltage. The X-ray pulse widths were about 300 ns, and the time-integrated X-ray intensity measured by a thermoluminescence dosimeter (Kyokko TLD Reader 1500 having MSO-S elements without energy compensation) had a value of about 1.0 mGy at 1.0 m from the X-ray source with a charging voltage of 50 kV.

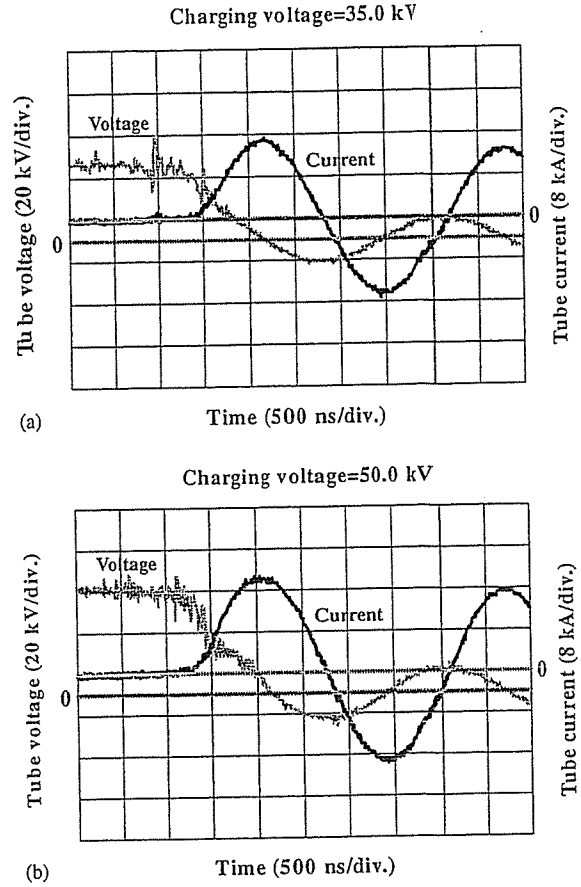

Fig. 3. Tube voltages and currents with a charging voltage of (a) 35.0 kV and (b) 50.0 kV.

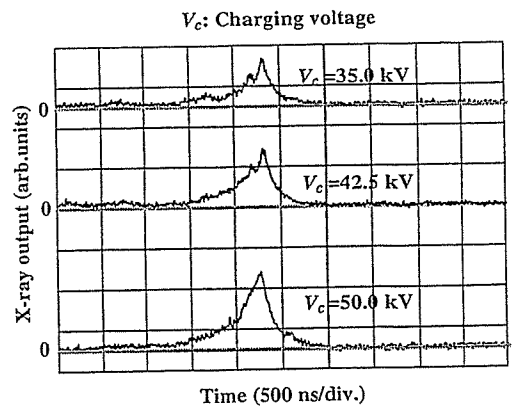

Fig. 4. X-ray outputs at the indicated conditions.

3.3. X-ray source

In order to roughly observe images of the plasma X-ray source in the detector plane, we employed a pinhole camera with a hole diameter of 100 μm (Fig. 5). When

the charging voltage was increased, the plasma X-ray source grew, and both spot dimension and intensity increased. Because the X-ray intensity is the highest at the center of the spot, both the dimension and intensity decreased according to both increases in the thickness of a filter for absorbing X-rays and decreases in the pinhole diameter.

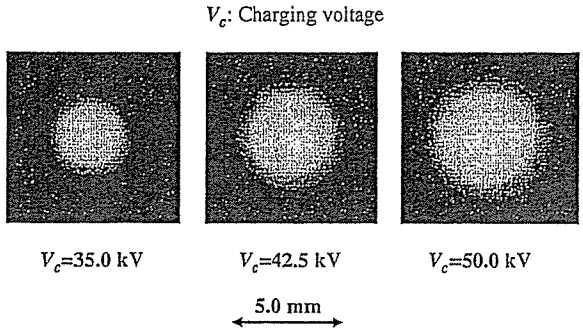

Fig. 5. Images of plasma X-ray source.

3.4. X-ray spectra

X-ray spectra from the plasma source were measured by a transmission-type spectrometer with a lithium fluoride curved crystal 0.5 mm in thickness. The spectra were taken by a computed radiography (CR) system (Sato et al., 2000) (Konica Minolta Regius 150) with a wide dynamic range, and relative X-ray intensity was calculated from Dicom digital data. Subsequently, the relative X-ray intensity as a function of the data was calibrated using a conventional X-ray generator, and we confirmed that the intensity was proportional to the

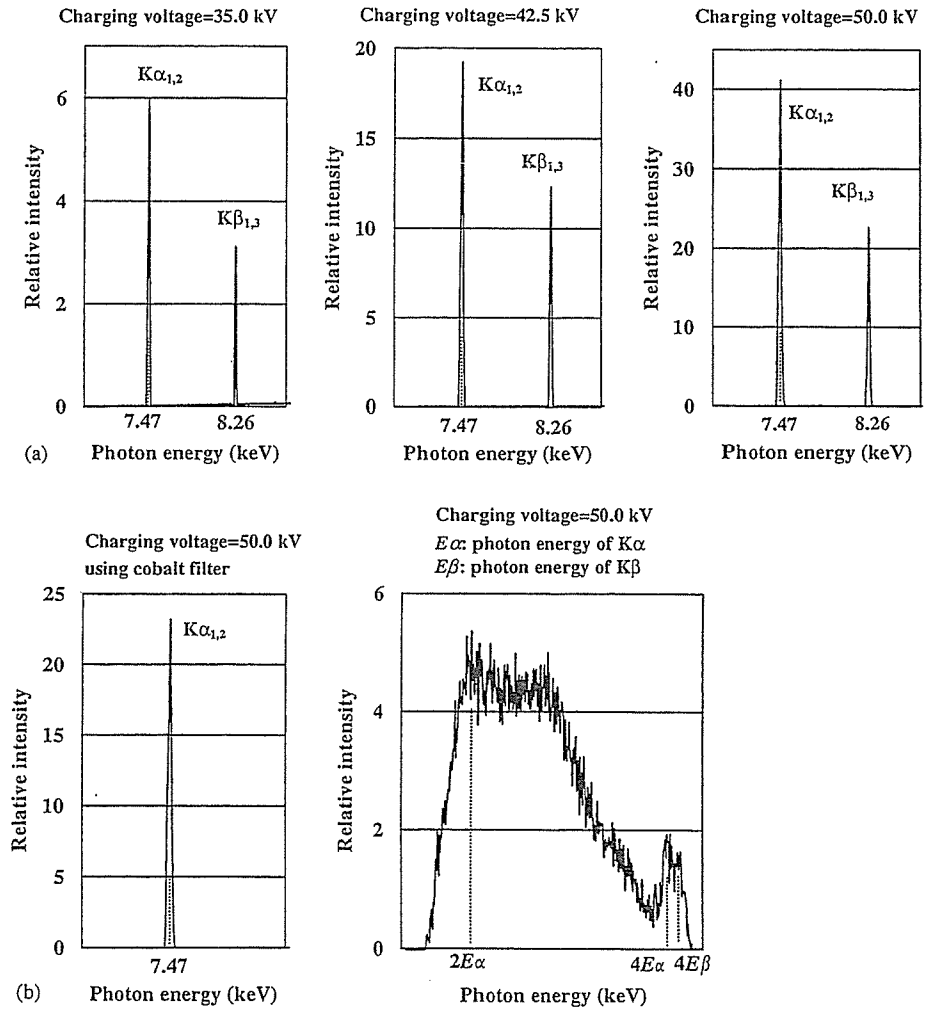

Fig. 6. X-ray spectra from weakly ionized nickel plasma at the indicated conditions. (a) Kα and Kβ rays and (b) Kα and higher harmonic rays.

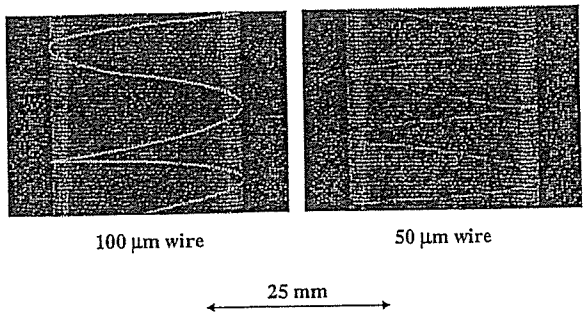

Fig. 7. Radiograms of tungsten wires coiled around PMMA pipes.

exposure time. Fig. 6 shows measured spectra from the copper target with a charging voltage of 50 kV. In fact, we observed clean K lines such as lasers, and Kα lines were left by absorbing Kβ lines using a 15-μm-thick cobalt filter. The characteristic X-ray intensity substantially increased with corresponding increases in the charging voltage, and higher harmonic hard X-rays were observed.

4. Radiography

The plasma radiography was performed by the CR system without using the filter. The charging voltage and the distance between the X-ray source and imaging plate were 50 kV and 1.2 m, respectively.

Firstly, rough measurements of spatial resolution were made using wires. Fig. 7 shows radiograms of tungsten wires coiled around pipes made of polymethyl methacrylate (PMMA). Although the image contrast decreased somewhat with decreases in the wire diameter, due to blurring of the image caused by the sampling pitch of 87.5 μm, a 50-μm-diameter wire could be observed.

Fig. 8 shows a radiogram of a vertebra, and fine structures in the vertebra were observed. Next, an image of plastic bullets falling into a polypropylene beaker from a plastic test tube is shown in Fig. 9. Because the X-ray duration was about 500 ns, the stop-motion image of bullets could be obtained.

5. Conclusions and outlook

Concerning the spectrum measurement, we obtained fairly intense and clean K lines from a weakly ionized linear plasma X-ray source, and Kα lines were left by absorbing Kβ lines using the cobalt filter. In particular, the higher harmonic X-rays were produced from the plasma. Because the X-ray intensities of the harmonics increased with increases in the charging voltage, the

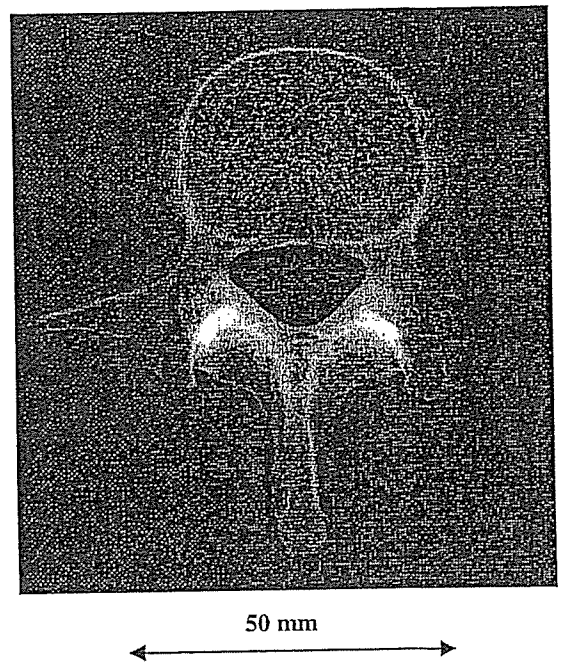

Fig. 8. Radiogram of a vertebra.

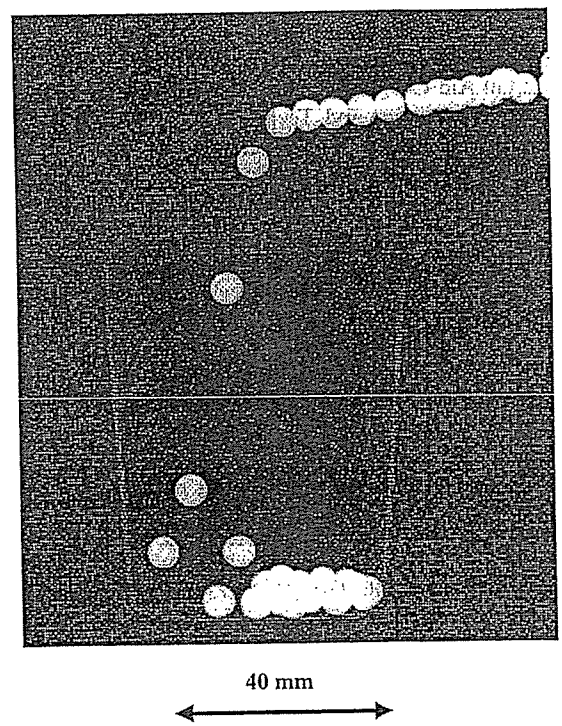

Fig. 9. Radiogram of plastic bullets falling into polypropylene beaker from a plastic test tube.

harmonic bremsstrahlung rays survived due to the X-ray resonation.

To perform monochromatic radiography, the higher harmonics are not necessary. Therefore, the condenser charging voltage should be minimized in order to decrease the intensities of higher harmonics, and the condenser capacity should be maximized to increase the characteristic X-ray intensity. On the other hand, because the intensities of harmonics increase with increases in the charging voltage, high-photon-energy monochromatic radiography may be realized.

In this research, we obtained sufficient characteristic X-ray intensity per pulse for CR radiography, and the generator produced number of characteristic K photons was approximately 1×10^8 photons/cm^2 at 1.0 m per pulse. In addition, since the photon energy of characteristic X-rays can be controlled by changing the target elements, various quasi-monochromatic high-speed radiographies, such as high-contrast angiography and mammography, will be possible.

Acknowledgments

This work was supported by Grants-in-Aid for Scientific Research (13470154, 13877114, 16591181, and 16591222) and Advanced Medical Scientific Research from MECSST, Health and Labor Sciences Research Grants (RAMT-nano-001, RHGTEFB-genome-005 and RHGTEFB-saisei-003), Grants from the Keiryo Research Foundation, the Promotion and Mutual Aid Corporation for Private Schools of Japan, the Japan Science and Technology Agency (JST), and the New Energy and Industrial Technology Development Organization (NEDO, Industrial Technology Research Grant Program in '03).

References

Ando, M., Maksimenko, M., Sugiyama, H., Pattanasiriwisawa, W., Hyodo, K., Uyama, C., 2002. A simple X-ray dark- and bright- field imaging using achromatic Laue optics. Jpn J. Appl. Phys. 41, L1016–L1018.

Davis, T.J., Gao, D., Gureyev, T.E., Stevenson, A.W., Wilkins, S.W., 1995. Phase-contrast imaging of weakly absorbing materials using hard X-rays. Nature 373, 595–597.

Germer, R., 1979. X-ray flash techniques. J. Phys. E: Sci. Instrum. 12, 336–350.

Hyodo, K., Ando, M., Oku, Y., Yamamoto, S., Takeda, T., Itai, Y., Ohtsuka, S., Sugishita, Y., Tada, J., 1998. Development of a two-dimensional imaging system for clinical applications of intravenous coronary angiography using intense synchrotron radiation produced by a multipole wiggler. J. Synchrotron. Rad. 5, 1123–1126.

Macchietto, C.D., Benware, B.R., Rocca, J.J., 1999. Generation of millijoule-level soft-X-ray laser pulses at a 4-Hz repetition rate in a highly saturated tabletop capillary discharge amplifier. Opt. Lett. 24, 1115–1117.

Momose, A., Takeda, T., Itai, Y., Hirano, K., 1996. Phase-contrast X-ray computed tomography for observing biological soft tissues. Nat. Med. 2, 473–475.

Mori, H., Hyodo, K., Tanaka, E., Mohammed, M.U., Yamakawa, A., Shinozaki, Y., Nakazawa, H., Tanaka, Y., Sekka, T., Iwata, Y., Honda, S., Umetani, K., Ueki, H., Yokoyama, T., Tanioka, K., Kubota, M., Hosaka, H., Ishizawa, N., Ando, M., 1996. Small-vessel radiography in situ with monochromatic synchrotoron radiation. Radiology 201, 173–177.

Rocca, J.J., Shlyaptsev, V., Tomasel, F.G., Cortazar, O.D., Hartshorn, D., Chilla, J.L.A., 1994. Demonstration of a discharge pumped table-top soft X-ray laser. Phys. Lev. Lett. 73, 2192–2195.

Rocca, J.J., Clark, D.P., Chilla, J.L.A., Shlyaptsev, V.N., 1996. Energy extraction and achievement of the saturation linit in a discharge-pumped table-top soft X-ray amplifier. Phys. Lev. Lett. 77, 1476–1479.

Sato, E., Kimura, S., Kawasaki, S., Isobe, H., Takahashi, K., Tamakawa, Y., Yanagisawa, T., 1990. Repetitive flash X-ray generator utilizing a simple diode with a new type of energy-selective function. Rev. Sci. Instrum. 61, 2343–2348.

Sato, E., Takahashi, K., Sagae, M., Kimura, S., Oizumi, T., Hayasi, Y., Tamakawa, Y., Yanagisawa, T., 1994a. Sub-kilohertz flash X-ray generator utilizing a glass-enclosed cold-cathode triode. Med. Biol. Eng. Comput. 32, 289–294.

Sato, E., Sagae, M., Takahashi, K., Shikoda, A., Oizumi, T., Hayasi, Y., Tamakawa, Y., Yanagisawa, T., 1994b. 10 kHz microsecond pulsed X-ray generator utilizing a hot-cathode triode with variable durations for biomedical radiography. Med. Biol. Eng. Comput. 32, 295–301.

Sato, E., Sato, K., Tamakawa, Y., 2000. Film-less computed radiography system for high-speed imaging. Ann. Rep. Iwate Med. Univ. Sch. Lib. Arts Sci. 35, 13–23.

Sato, E., Hayasi, Y., Germer, R., Tanaka, E., Mori, H., Kawai, T., Obara, H., Ichimaru, T., Takayama, K., Ido, H., 2003a. Irradiation of intense characteristic X-rays from weakly ionized linear molybdenum plasma. Jpn J. Med. Phys. 23, 123–131.

Sato, E., Hayasi, Y., Germer, R., Tanaka, E., Mori, H., Kawai, T., Ichimaru, T., Takayama, K., Ido, H., 2003b. Quasi-monochromatic flash X-ray generator utilizing weakly ionized linear copper plasma. Rev. Sci. Instrum. 74, 5236–5240.

Sato, E., Sagae, M., Tanaka, E., Hayasi, Y., Germer, R., Mori, H., Kawai, T., Ichimaru, T., Sato, S., Takayama, Y., Ido, H., 2004a. Quasi-monochromatic flash X-ray generator utilizing a disk-cathode molybdenum tube. Jpn J. Appl. Phys. 43, 7324–7328.

Sato, E., Hayasi, Y., Germer, R., Tanaka, E., Mori, H., Kawai, T., Ichimaru, T., Sato, S., Takayama, K., Ido, H., 2004b. Sharp characteristic X-ray irradiation from weakly ionized linear plasma. J. Electron. Spectrosc. Related Phenom. 137–140, 713–720.

Sato, E., Tanaka, E., Mori, H., Kawai, T., Ichimaru, T., Sato, S., Takayama, K., Ido, H., 2004c. Demonstration of

enhanced K-edge angiography using a cerium target X-ray generator. Med. Phys. 31, 3017–3021.

Sato, E., Tanaka, E., Mori, H., Kawai, T., Ichimaru, T., Sato, S., Takayama, Y., Ido, H., 2005a. Compact monochromatic flash X-ray generator utilizing a disk-cathode molybdenum tube. Med. Phys. 32, 49–54.

Sato, E., Tanaka, E., Mori, H., Kawai, T., Sato, S., Takayama, Y., 2005b. High-speed enhanced K-edge angiography utilizing cerium plasma X-ray generator. Opt. Eng. 44, 049001–049016.

Sato, E., Tanaka, E., Mori, H., Kawai, T., Sato, S., Takayama, Y., 2005c. Clean monochromatic X-ray irradiation from weakly ionized linear copper plasma. Opt. Eng. 44, 049002–049016.

Shikoda, A., Sato, E., Sagae, M., Oizumi, T., Tamakawa, Y., Yanagisawa, T., 1994. Repetitive flash X-ray generator having a high-durability diode driven by a two-cable-type line pulser. Rev. Sci. Instrum. 65, 850–856.

Takahashi, K., Sato, E., Sagae, M., Oizumi, T., Tamakawa, Y., Yanagisawa, T., 1994. Fundamental study on a long-duration flash X-ray generator with a surface-discharge triode. Jpn J. Appl. Phys. 33, 4146–4151.

Thompson, A.C., Zeman, H.D., Brown, G.S., Morrison, J., Reiser, P., Padmanabahn, V., Ong, L., Green, S., Giacomini, J., Gordon, H., Rubenstein, E., 1992. First operation of the medical research facility at the NSLS for coronary angiography. Rev. Sci. Instrum. 63, 625–628.

Available online at www.sciencedirect.com
ScienceDirect
Radiation Physics and Chemistry 75 (2006) 2008–2013
Radiation Physics and Chemistry
www.elsevier.com/locate/radphyschem

Tunable narrow-photon-energy X-ray generator utilizing a tungsten-target tube

Eiichi Sato[a,*], Hiroshi Sugiyama[b], Masami Ando[b], Etsuro Tanaka[c], Hidezo Mori[d], Toshiaki Kawai[e], Takashi Inoue[f], Akira Ogawa[f], Kazuyoshi Takayama[g], Jun Onagawa[h], Hideaki Ido[h]

[a]*Department of Physics, Iwate Medical University, 3-16-1 Honchodori, Morioka 020-0015, Japan*
[b]*Photon Factory, Institute of Materials Structure Science, High Energy Accelerator Research Organization, 1-1 Oho, Tsukuba 305-0801, Japan*
[c]*Department of Nutritional Science, Faculty of Applied Bio-science, Tokyo University of Agriculture, 1-1-1 Sakuragaoka, Setagaya-ku 156-8502, Japan*
[d]*Department of Cardiac Physiology, National Cardiovascular Center Research Institute, 5-7-1 Fujishirodai, Suita, Osaka 565-8565 Japan*
[e]*Electron Tube Division #2, Hamamatsu Photonics K.K., 314-5 Shimokanzo, Iwata 438-0193, Japan*
[f]*Department of Neurosurgery, School of Medicine, Iwate Medical University, 19-1 Uchimaru, Morioka 020-8505, Japan*
[g]*Shock Wave Research Center, Institute of Fluid Science, Tohoku University, 2-1-1 Katahira, Sendai 980-8577, Japan*
[h]*Department of Applied Physics and Informatics, Faculty of Engineering, Tohoku Gakuin University, 1-13-1 Chuo, Tagajo 985-8537, Japan*

Accepted 23 November 2005

Abstract

A preliminary experiment for producing narrow-photon-energy cone-beam X-rays using a silicon single crystal is described. In order to produce low-photon-energy X-rays, a 100-μm-focus X-ray generator in conjunction with a (1 1 1) plane silicon crystal is employed. The X-ray generator consists of a main controller and a unit with a high-voltage circuit and a microfocus X-ray tube. The maximum tube voltage and current were 35 kV and 0.50 mA, respectively, and the X-ray intensity of the microfocus generator was 48.3 μGy/s at 1.0 m from the source with a tube voltage of 30 kV and a current of 0.50 mA. The effective photon energy is determined by Bragg's angle, and the photon-energy width is regulated by the angle delta. Using this generator in conjunction with a computed radiography system, quasi-monochromatic radiography was performed using a cone beam with an effective energy of approximately 17 keV.

PACS: 87.59.–e; 87.59.Bh; 87.64.Gb

Keywords: Narrow-photon-energy X-rays; Tunable photon energy; Silicon single crystal; Cone beam

1. Introduction

Since the birth of the synchrotron, monochromatic parallel X-ray beams have been applied to X-ray phase-contrast radiography (Davis et al., 1995; Momose et al.,

*Corresponding author.
E-mail address: dresato@iwate-med.ac.jp (E. Sato).

0969-806X/$ - see front matter © 2006 Elsevier Ltd. All rights reserved.
doi:10.1016/j.radphyschem.2005.11.019

1996; Ando et al., 2002) and enhanced K-edge angiography (Thompson et al., 1992; Mori et al., 1996; Hyodo et al., 1998). The phase imaging is primarily based on the X-ray refraction, and the angiography is performed using X-rays with a photon energy of just beyond the K-absorption edge of iodine.

In order to perform high-speed medical radiography, although several different flash X-ray generators utilizing cold-cathode tubes have been developed (Sato et al., 1990, 1994a, b; Shikoda et al., 1994; Takahashi et al., 1994), quasi-monochromatic flash X-ray generators (Sato et al., 2003a, b, 2004a, b, 2005a–c) are useful to produce clean K-series characteristic X-rays without using a filter. Therefore, we have performed a demonstration of cone-beam K-edge angiography utilizing a cerium plasma generator, since K-series characteristic X-rays from the cerium target are absorbed effectively by iodine. In view of this situation, we have developed a steady state X-ray generator utilizing a cerium-target tube (Sato et al., 2004c), and have demonstrated enhanced K-edge angiography utilizing cerium Kα lines.

Without using synchrotrons, X-ray phase-contrast radiography for edge enhancement has been performed using a microfocus X-ray tube (Wilkins et al., 1996), and the digital imaging achieved with a 100-μm-focus molybdenum tube has been applied effectively to perform mammography (Ishisaka et al., 2000).

In this paper, we present a tunable narrow-photon-energy X-ray generator utilizing a single silicon crystal, and examine its suitability for energy-selective cone-beam radiography.

2. Experimental setup

Fig. 1 shows the block diagram of the X-ray generator, which consists of a main controller and an X-ray tube unit with a Cockcroft–Walton circuit and a 100-μm-focus X-ray tube. The tube voltage, the current, and the exposure time can be controlled by the controller. The main circuit for producing X-rays is illustrated in Fig. 2, and employed the Cockcroft–Walton circuit in order to decrease the dimensions of the tube unit. In the X-ray tube, positive and negative high voltages are applied to the anode and cathode electrodes, respectively. The filament heating current is supplied by an AC power supply in the controller in conjunction with an insulation transformer. The maximum tube voltage and current of the generator are 105 kV and 0.50 mA, respectively. In this experiment, the tube voltage applied was from 18 to 34 kV, and the tube current was 0.50 mA (maximum current) by the filament temperature. The exposure time is controlled in order to obtain optimum X-ray intensity.

The narrow-photon-energy X-ray generator utilizing a single silicon crystal of (1 1 1) plane is shown in Fig. 3. The effective photon energy is determined by Bragg's angle, and the photon-energy width is regulated by the

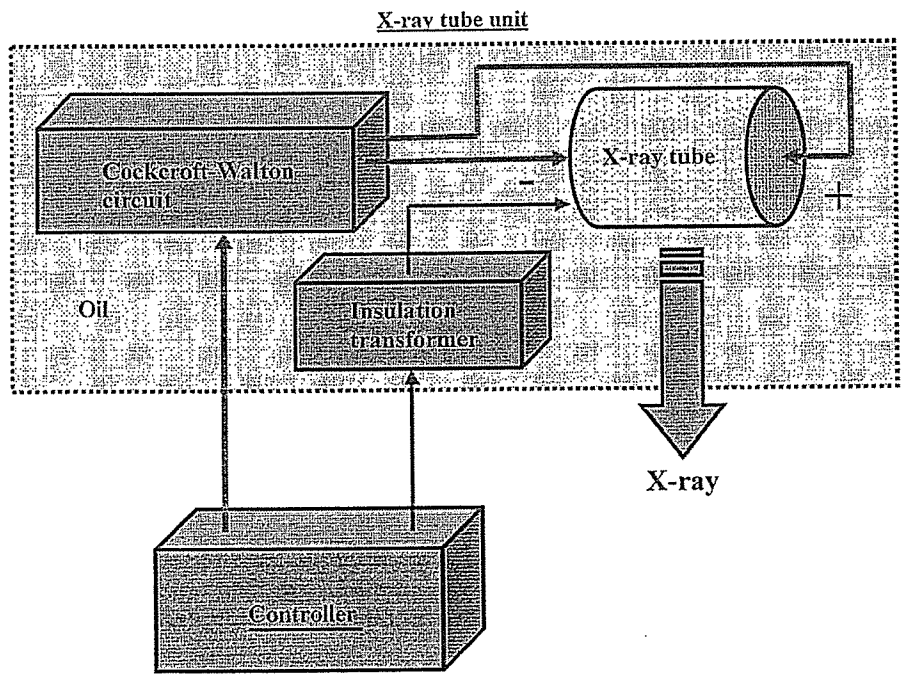

Fig. 1. Block diagram of a compact 100-μm focus X-ray generator with a tungsten-target radiation tube.